

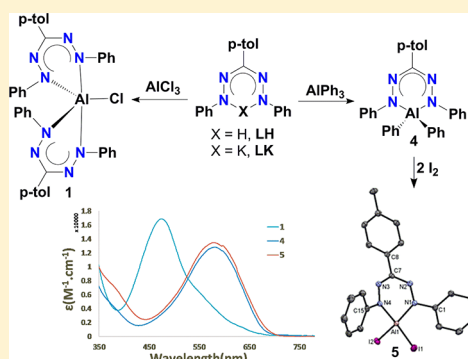
## Aluminum Complexes with Redox-Active Formazanate Ligand: Synthesis, Characterization, and Reduction Chemistry

Ranajit Mondol and Edwin Otten\*<sup>✉</sup>

Stratingh Institute for Chemistry, University of Groningen, Nijenborgh 4, 9747 AG Groningen, The Netherlands

### Supporting Information

**ABSTRACT:** The synthesis of aluminum complexes with redox-active formazanate ligands is described. Salt metathesis using  $\text{AlCl}_3$  was shown to form a five-coordinate complex with two formazanate ligands, whereas organometallic aluminum starting materials yield tetrahedral mono-(formazanate) aluminum compounds. The aluminum diphenyl derivative was successfully converted to the iodide complex (formazanate) $\text{AlI}_2$ , and a comparison of spectroscopic/structural data for these new complexes is provided. Characterization by cyclic voltammetry is supplemented by chemical reduction to demonstrate that ligand-based redox reactions are accessible in these compounds. The possibility to obtain a formazanate aluminum(I) carbenoid species by two-electron reduction was examined by experimental and computational studies, which highlight the potential impact of the nitrogen-rich formazanate ligand on the electronic structure of compounds with this ligand.



### INTRODUCTION

Aluminum is one of the most abundant elements in the earth's crust and is used in a large variety of applications: the metal itself is ductile, lightweight, and corrosion resistant, and it can form various alloys to improve its mechanical properties. Molecular compounds containing aluminum are also widespread: aluminum halides are strong Lewis acid catalysts for Friedel–Crafts reactions, and organometallic derivatives are used in Ziegler–Natta polymerization of olefins.<sup>1</sup> The vast majority of aluminum compounds that are known today contain aluminum in the most stable +3 oxidation state. However, complexes of aluminum (and other group 13 elements) in lower oxidation states have recently attracted significant attention for their unusual (transition-metal-like) reactivity<sup>2,3</sup> and novel bonding motifs (e.g., clusters,<sup>4</sup> multiply bonded compounds).<sup>5</sup>

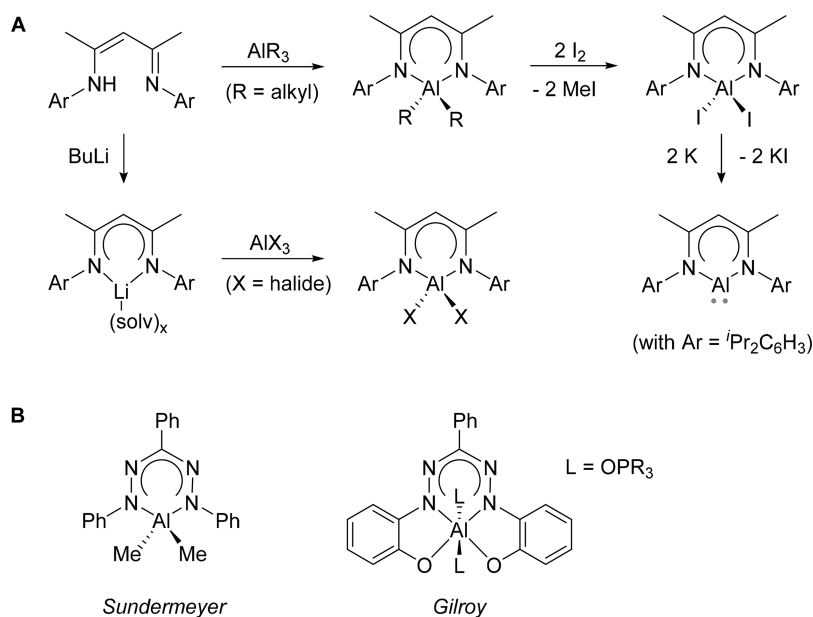
Compounds of aluminum with the well-known  $\beta$ -diketiminate ligands have been prepared by alkane elimination (from trialkyl aluminums) or by salt metathesis reactions (using aluminum halides, Scheme 1A). Given the ease of preparation of these ligands and their tunable steric and electronic properties, complexes of this type have been studied in a variety of transformations. For example,  $\beta$ -diketiminate aluminum dialkyls react with strong Lewis acids to form three-coordinate cationic derivatives,<sup>6</sup> which show reversible cycloaddition of ethylene,<sup>7,8</sup> and these and related cationic aluminum species with anionic bidentate N-ligands have been applied in catalytic reactions that make use of their high Lewis acidity.<sup>9,10</sup> Neutral  $\beta$ -diketiminate aluminum complexes with various coligands (e.g., halides,<sup>11</sup> alkyls,<sup>12–14</sup> amides,<sup>14</sup> hydroxides)<sup>15–19</sup> have also been prepared, and their reactivity

in ring-opening polymerization of cyclic esters was investigated.<sup>13,20,21</sup> The majority of these studies employ  $\beta$ -diketiminate ligands with sterically demanding N–Ar substituents (e.g., Ar = 2,6-*i*-Pr<sub>2</sub>C<sub>6</sub>H<sub>3</sub>) that shield the Al center, but recently derivatives with less bulky groups were described.<sup>22–24</sup> An unusual low-valent aluminum(I) compound with sterically demanding  $\beta$ -diketiminate ligand was prepared by Roesky and co-workers via potassium reduction of the diiodide complex (Scheme 1A).<sup>25</sup>

In contrast to the rich chemistry reported for aluminum complexes with  $\beta$ -diketiminate ligands, comparatively little is known about the related ligands with two additional nitrogen atoms in the ligand backbone (N<sub>2</sub>CNN, i.e., formazanates). Sundermeyer and co-workers have reported the synthesis and characterization of a series of group 13 formazanate dialkyl complexes,<sup>26</sup> and Gilroy et al. described six-coordinate Al complexes with formazanate-based trianionic N<sub>2</sub>O<sub>2</sub> ligands<sup>27</sup> (Scheme 1B). After Hicks' initial observation of facile ligand-based reductions in a main group compound with a redox-active formazanate ligand,<sup>28</sup> our group<sup>29–34</sup> as well as the Gilroy group<sup>27,35–42</sup> have in the last years developed formazanate chemistry with the lightest group 13 element boron. During our studies of the reduction chemistry, we found that 2-electron reduction of a formazanate boron difluoride compound generates a series of BN-heterocycles that originate from a putative (formazanate)B carbenoid intermediate.<sup>32</sup> In recent years, several examples of isolable main group compounds in reduced states have been

Received: February 26, 2019

Published: April 12, 2019

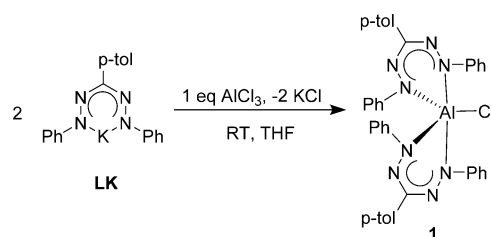
Scheme 1. (A) Synthesis of Aluminum Complexes with  $\beta$ -Diketiminato Ligands and (B) Aluminum Complexes with Formazanate Ligands

discovered, and the activation of unreactive bonds by these compounds (e.g., via oxidative addition) is being developed.<sup>3,43,44</sup>

Given our interest in using redox-active ligands to manipulate electronic structure and stabilize compounds in unusual oxidation states, we set out to explore the synthesis of aluminum complexes with formazanate ligands. In this paper, we provide spectroscopic and crystallographic characterization data for mono- and bis-formazanate aluminum complexes and their electrochemistry. The reduction chemistry of these compounds is described, and the experimental data are supported by a computational (DFT) study.

## RESULT AND DISCUSSION

**Synthesis of Formazanate Aluminum Complexes.** Salt metathesis reactions<sup>11,12</sup> were initially evaluated as a route to obtain mono(formazanate) aluminum dihalide complexes, which could subsequently serve as synthons for low-valent Al compounds. Thus, a suspension of  $\text{AlCl}_3$  in  $\text{THF-}d_8$  was treated in an NMR tube with 1 equiv of the potassium formazanate salt  $\text{K}[\text{PhNNC}(p\text{-tol})\text{NNPh}] \cdot 2\text{THF}$  (**LK**),<sup>45</sup> resulting in a rapid color change from purple to dark red. The  $^1\text{H}$  NMR spectrum of this solution showed diagnostic resonances for the *p*-tolyl and phenyl moieties in a 1:2 ratio that were shifted from the starting material, indicating the formation of a new formazanate aluminum complex. On preparative scale, **1** could be obtained as crystalline material in moderate yield (36%) by diffusion of hexane into a THF solution of the product (Scheme 2). A single-crystal X-ray structure determination showed that instead of the desired mono(formazanate)aluminum complex the product is bis(formazanate) complex  $[\text{PhNNC}(p\text{-tol})\text{NNPh}]_2\text{AlCl}$  (**1**) (Figure 1, pertinent bond lengths and angles are presented in Table 1) in which the Al center is bound to two bidentate formazanate ligands. The coordination sphere is complemented by a chloride ligand, resulting in a five-coordinate Al(III) complex. The geometry around the Al center is best described as a distorted trigonal bipyramid ( $\tau = 0.6353$ ),<sup>46</sup>

Scheme 2. Synthesis of Bis(formazanate) Aluminum Chloride Compound **1**

with a bond angle between the “axial” Al–N bonds (N1–Al1–N8) of  $165.22(1)^\circ$ .

The Al center is significantly displaced out of the planes defined by formazanate NNNN backbones (displacement from N1–N4/N5–N8 planes is 1.068/1.058 Å, respectively). The molecular structure of **1** reveals that the Al–N1 and Al–N8 bond vectors lie along the axial directions and the Al–Cl1, Al–N4, and Al–N5 bonds form the equatorial plane in **1** (Figure 1). The axial Al–N bonds are elongated as compared to equatorial Al–N bonds by about 0.081 Å, similar to related pentacoordinated Al(III) compounds in the literature,<sup>47,48</sup> and both are significantly longer than the Al–N bonds in four-coordinate  $\beta$ -diketiminato aluminum dichlorides.<sup>11</sup> The Al–Cl bond length in **1** (2.143(1) Å) is somewhat shorter than that in Berben’s pentacoordinated aluminum chloride complex with two bidentate nitrogen ligands (2.191(1) Å).<sup>47</sup>

The room-temperature  $^1\text{H}$  NMR spectrum of **1** reveals only one set of signals for the NPh groups. The equivalence of the axial and equatorial positions is likely due to facile exchange via Berry pseudorotation.<sup>49</sup> The  $^{27}\text{Al}$  NMR of **1** shows a resonance at 43.0 ppm, which is in agreement with the presence of a pentacoordinated Al center in **1**.<sup>50–53</sup>

The cyclic voltammogram of compound **1** was measured in THF solution (Figure 2), which revealed two quasi-reversible 1-electron redox-events at  $-1.36$  and  $-1.67$  V vs  $\text{Fc}^{0/+}$ . These values are in a range similar to that of our previously published bis(formazanate)Zn compounds<sup>29,31</sup> and consistent with two

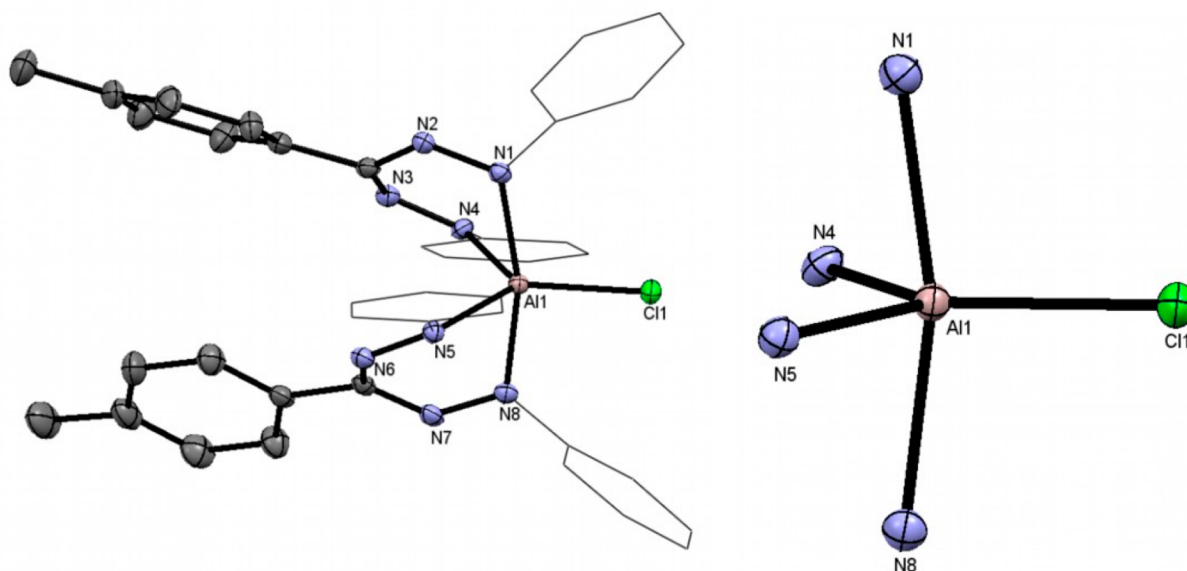


**Figure 1.** (a) Molecular structure of **1** showing 50% probability ellipsoids. Hydrogen atoms were omitted, and NPh groups are shown as wireframe for clarity. (b) Coordination sphere around Al center.

**Table 1.** Selected Bond Lengths (Å) and Bond Angles (deg) for **1**

bond lengths		bond angles	
Al1–Cl1	2.143(1)	N1–Al1–N8	165.22(1)
Al1–N1/Al1–N8	1.999(4)/2.007(4)	N1–Al1–Cl1/N8–Al1–Cl1	97.72(1)/97.03(1)
Al1–N4/Al1–N5	1.923(3)/1.921(3)	N1–Al1–N4/N8–Al1–N5	81.29(1)/81.89(1)
N1–N2/N7–N8	1.316(4)/1.307(4)	N1–Al1–N5/N8–Al1–N4	90.00(1)/89.18(1)
N3–N4/N5–N6	1.320(5)/1.322(4)	Cl1–Al1–N4/Cl1–Al1–N5	127.10(1)/126.25(1)
		N4–Al1–N5	106.65(1)

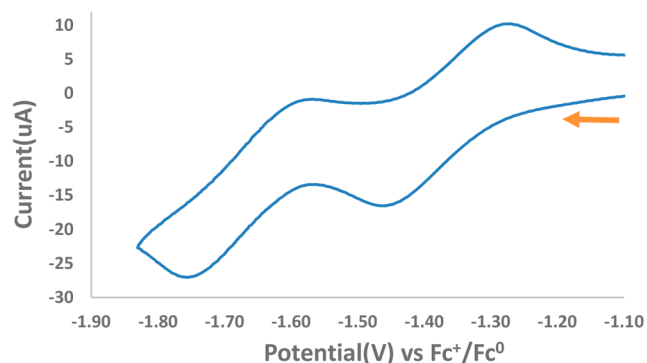
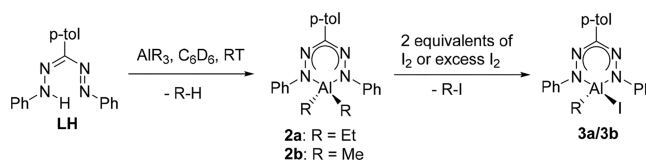


**Figure 2.** Cyclic voltammogram of **1** (1.5 mM solution in THF, 0.1 M [Bu<sub>4</sub>N][PF<sub>6</sub>]) recorded at 100 mVs<sup>-1</sup>.

independent, sequential 1-electron reduction processes for each ligand in compound **1**. Scanning toward more negative potentials resulted in several additional redox events below  $-1.9$ , which were not analyzed in detail (see Figure S1).

Given that straightforward salt metathesis reactions failed to give mono(formazanate) aluminum dihalides, we subsequently chose a two-step protocol based on the method of Roesky and co-workers for the synthesis of  $\beta$ -diketiminato aluminum diiodides.<sup>25</sup> Thus, the free formazan (**LH**) was treated with AlEt<sub>3</sub> in a 1:1 molar ratio in an NMR tube in C<sub>6</sub>D<sub>6</sub> (Scheme 3). As reported by Sundermeyer and co-workers for the aluminum methyl analogue,<sup>26</sup> this results in rapid formation of an intense blue solution for which the integrated intensities in

### Scheme 3. Synthesis of Dialkyl Aluminum Formazanate and (Monoiodo) (Monoalkyl) Aluminum Formazanate Compounds



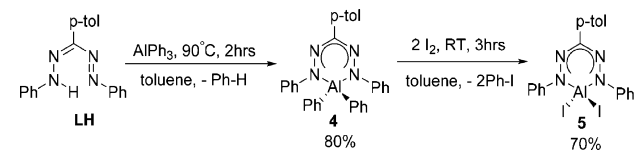
the <sup>1</sup>H NMR spectrum are in agreement with the presence of two AlEt groups per formazanate ligand.

The NMR data indicate that the product is the diethyl aluminum compound LAIEt<sub>2</sub> (**2a**). Compound **2a** is quite sensitive and is quickly hydrolyzed upon exposure to air. The high solubility of **2a** in common organic solvents rendered its purification by crystallization difficult. Treatment of *in situ* generated **2a** with 2 equiv of I<sub>2</sub> results in Et/I exchange as evidenced by the formation of EtI. However, the NMR spectrum indicates that only one AlEt group is replaced: One AlEt signal remains (AlCH<sub>2</sub> at 0.66 ppm), and the product is formulated as LAI(Et)I (**3a**). Longer reaction times as well as addition of more I<sub>2</sub> (additional 2 equiv) did not lead to further conversion by iodine exchange, indicating that it may be thermodynamically unfavorable to proceed beyond the monoethyl compound LAI(Et)I. Gently warming the NMR solution for 6 h to 40 °C did not indicate any further change, whereas decomposition was observed after 2 h at 70 °C. Testing AlMe<sub>3</sub> as the starting material suggested formation of

the mono(formazanate) aluminum dimethyl complex<sup>26</sup> but also for this compound iodine exchange only gave monoiodo product **3b** (Scheme 3).

Diphenyl derivative **4** (prepared from LH and AlPh<sub>3</sub>) could be obtained in crystalline form in 80% yield. The subsequent iodine exchange reaction was attempted by the reaction of 2 equiv of I<sub>2</sub> with **4** in an NMR tube in C<sub>6</sub>D<sub>6</sub>. In contrast to the dialkyl derivatives mentioned above, **4** cleanly converted to the desired aluminum diiodide [(PhNNC(*p*-tol)NNPh)AlI<sub>2</sub>] (**5**) as evidenced by the formation of 2 equiv of PhI and complete disappearance of the diagnostic resonances for the AlPh<sub>2</sub> moieties. On a preparative scale, **5** could be isolated as a crystalline material in good yield (70%) by slow diffusion of hexane into the reaction mixture in toluene (Scheme 4).

#### Scheme 4. Synthesis of Compounds **4** and **5**



Although the <sup>27</sup>Al NMR resonance of **4** could not be observed, diiodide analogue **5** shows a broad resonance at 69.50 ppm, consistent with a four-coordinated Al(III) center.<sup>12,54,55</sup> In the <sup>1</sup>H and <sup>13</sup>C NMR spectra, the presence of only one set of resonances for the N–Ph substituents of the ligand in **4** and **5** indicate that both molecules have (average) C<sub>2v</sub> symmetry in solution.

Single-crystal structure determinations for compounds **4** and **5** revealed the details of their molecular structures. A bidentate formazanate ligand is bound through its terminal N atoms forming a six-membered chelate ring, and the coordination sphere is complemented by two phenyl or iodide ligands, respectively (Figure 3). The overall geometries of **4** and **5** are distorted tetrahedral around the Al centers, which are displaced out of the plane composed by 4 N atoms from the ligand backbone by 0.531 and 0.419 Å, respectively. The smaller displacement for **5** is in accordance with less steric hindrance between the formazanate ligand and the Al substituents (I in **5** vs Ph in **4**). A similar trend for the

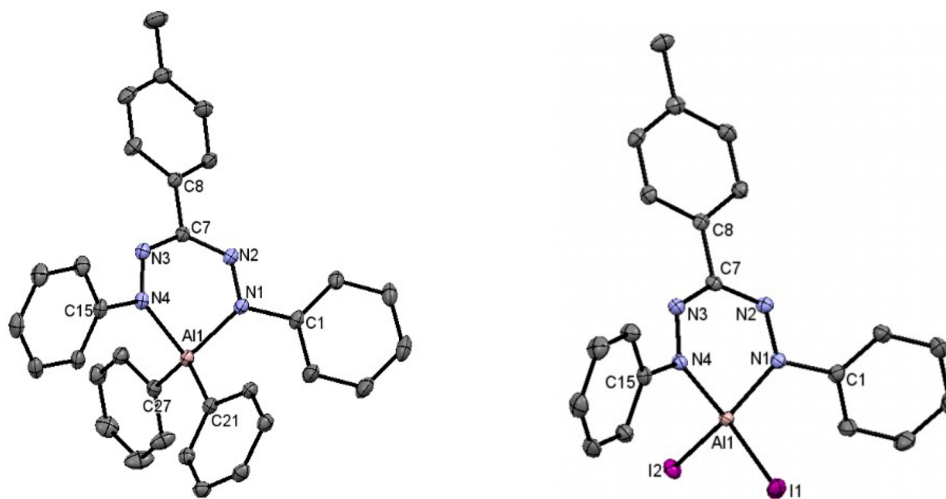
displacement of the Al center from the ligand plane was observed in related mono( $\beta$ -diketiminato) aluminum complexes.<sup>11,12</sup> The equivalent N–N and N–C bond distances support the presence of a delocalized ligand backbone in **4** and **5** (for selected bond lengths and bond angles, see Table 2).

**Table 2.** Selected Bond Lengths (Å) and Bond Angles (deg) for **4**, **4**<sup>2-</sup>, and **5**

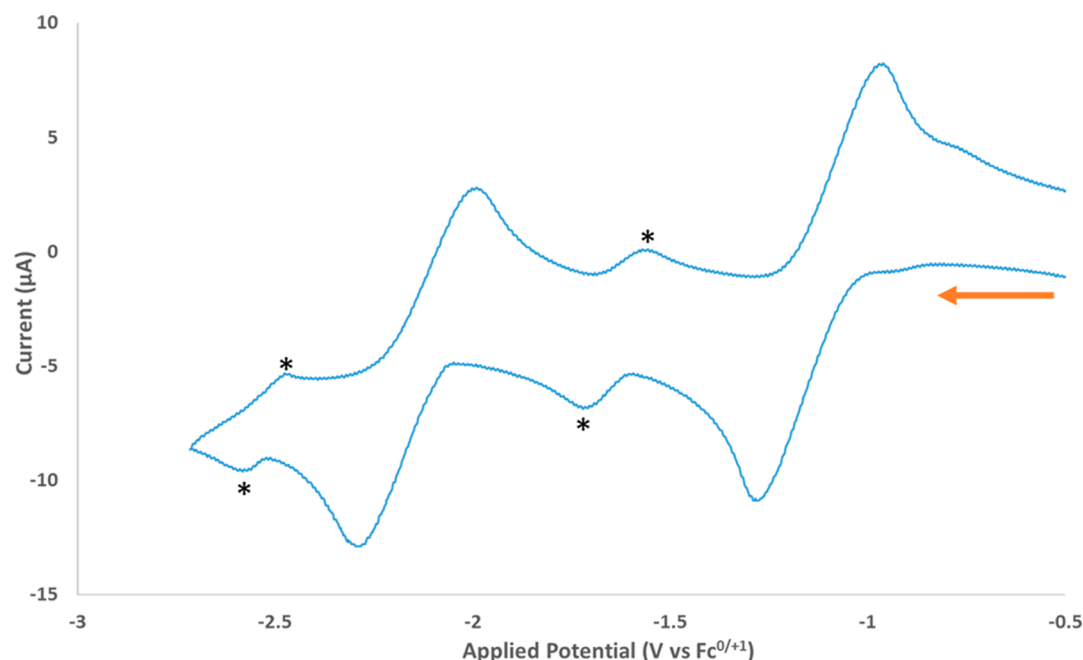
	<b>4</b>	<b>4</b> <sup>2-</sup>	<b>5</b>
Al1–N1	1.9336(9)	1.871(2)	1.893(2)
Al1–N4	1.9334(8)	1.873(2)	1.900(2)
Al–C21	1.962(1)	2.011(2)	
Al–C27	1.957(1)	2.011(2)	
Al–I1			2.497(7)
Al–I2			2.494(7)
N1–N2	1.315(1)	1.432(2)	1.317(2)
N2–C7	1.346(1)	1.332(2)	1.344(3)
C7–N3	1.347(1)	1.328(2)	1.346(3)
N3–N4	1.307(1)	1.432(2)	1.313(2)
N1–C1	1.433(1)	1.375(2)	
N4–C15	1.430(1)	1.371(3)	
N1–Al1–N4	90.01(4)	98.54(7)	92.83(8)

Similar bond distances were found in the corresponding tetra- and hexa-coordinated formazanate aluminum compounds reported by Sundermeyer et al.<sup>26</sup> and Gilroy et al.,<sup>27</sup> respectively. The Al–N bonds (1.893(2)–1.900(2) Å) in **5** are somewhat shorter than the Al–N bonds present in **4** (1.933(1)–1.934(1) Å), which could be attributed to the increased positive charge on Al center in **5** as iodide is more electron-withdrawing than a phenyl group.

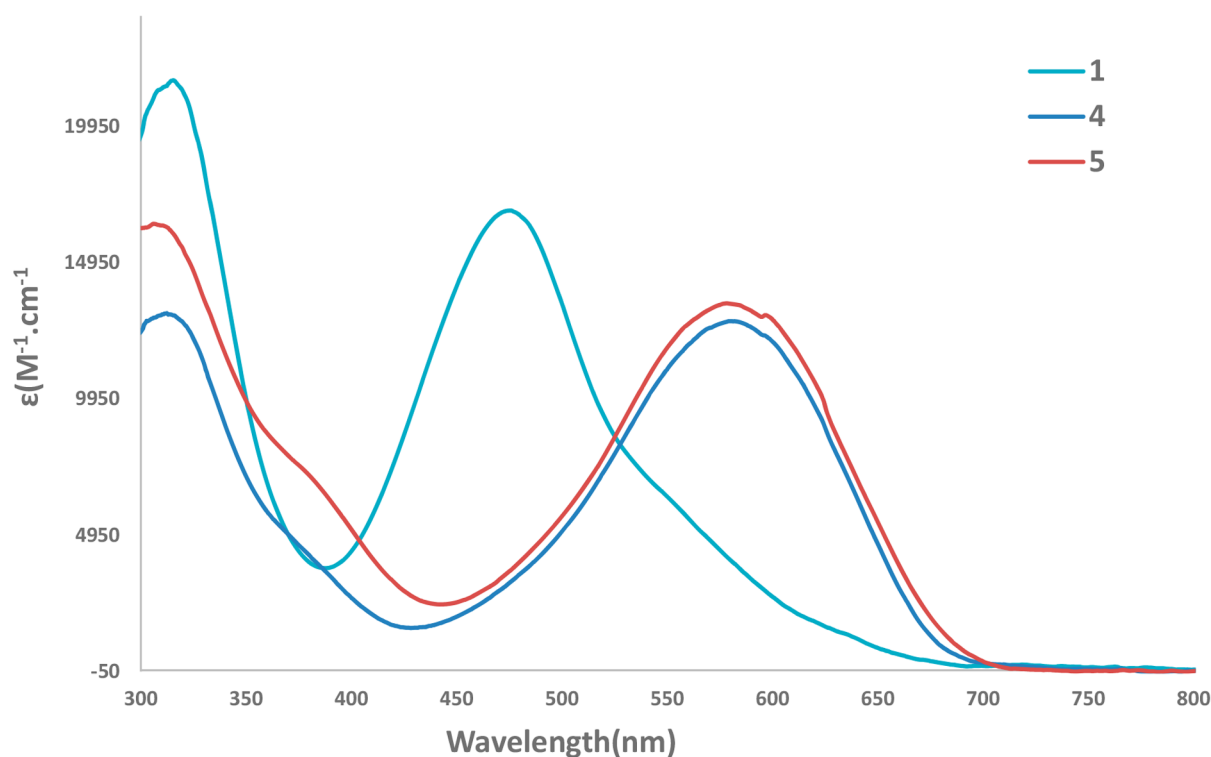
Cyclic voltammetry was employed to investigate the electrochemical properties of **4** and **5**. The voltammogram of **4** in THF solution (Figure 4) shows two quasi-reversible one-electron redox events at  $E^0 = -1.12$  and  $-2.13$  V vs Fc<sup>0/+1</sup> that correspond to two sequential ligand-based reductions to generate the radical anion **4**<sup>•-</sup> and the dianion **4**<sup>2-</sup>. In comparison to the boron analogue, these redox-potentials are shifted toward positive potential by 130 and 230 mV, respectively.<sup>34</sup> In contrast to the data for the diphenyl complex **4**, the voltammogram of the aluminum iodide **5** measured in



**Figure 3.** Molecular structures of **4** (left) and **5** (right) showing 50% probability ellipsoids. Hydrogen atoms are omitted for clarity.



**Figure 4.** Cyclic voltammetry of **4** (1.5 mM solution in THF, 0.1 M  $[\text{Bu}_4\text{N}][\text{PF}_6]$ ) recorded at  $100 \text{ mV s}^{-1}$ . Asterisks indicate redox-events due to a small amount of free ligand which is either present in the sample or generated in THF from **4** (see Figures S2–S4).

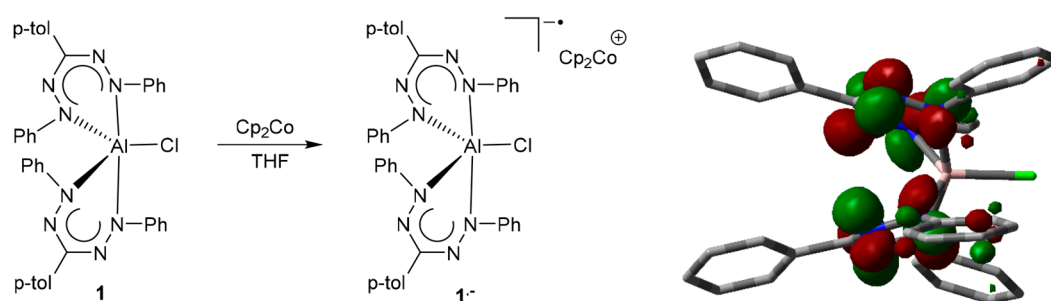


**Figure 5.** Absorption spectra of compounds **1**, **4**, and **5** in toluene.

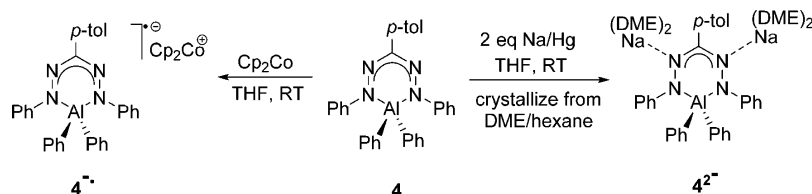
either THF or DME solution is poorly reversible and shows reduction events that are shifted to more negative potentials (see the [Supporting Information](#)). The changes in electrochemistry upon changing the Al-substituents from Ph to I may reflect the lability of the Al–I bond upon reduction.

The UV/vis absorption spectra were recorded for compounds **1**, **4**, and **5** in toluene solution to obtain more insight into the electronic properties for these compounds. All three

compounds show intense absorption maxima in the visible range of the spectrum, with extinction coefficients that range between  $13\,000$  and  $16\,800 \text{ L}\cdot\text{mol}^{-1}\cdot\text{cm}^{-1}$ , which are assigned to  $\pi\text{--}\pi^*$  transitions within the formazanate ligand backbone (Figure 5).<sup>26,27</sup> Bis(formazanate) complex **1** shows a broad absorption band at  $478 \text{ nm}$  with a shoulder toward lower energy. The absorption maximum for **1** is hypsochromically shifted by ca.  $10 \text{ nm}$  with respect to that of the free formazan

Scheme 5. Compound **1**<sup>a</sup>

<sup>a</sup>Reduction of compound **1** (left) and SOMO of **1**<sup>•-</sup> (right).

Scheme 6. Synthesis of 1- and 2-Electron-Reduced Derivatives of **4**

(488 nm in  $\text{CHCl}_3$ ,<sup>27</sup> 490 nm in hexane).<sup>26</sup> This stands in marked contrast to the bathochromic shift that is typically observed in formazanate complexes, a feature that has been ascribed to the anionic nature of the ligand and its increased rigidity upon complexation.<sup>27</sup> A reason for this discrepancy likely lies in the way the metal center is incorporated in the six-membered chelate structure: Other mono(formazanate) aluminum complexes have more planar  $\text{AlN}_4\text{C}$  rings, providing an extended conjugated  $\pi$ -system that includes the  $\text{N}-\text{Ar}$  groups. In contrast, the presence of two formazanate ligands in **1** enforces a strong “butterfly” distortion of the chelate ring in which the Al center is  $>1$  Å displaced from the coordination plane, and disrupts conjugation with the  $\text{N}-\text{Ph}$  groups.

Mono(formazanate) compounds **4** and **5** have very similar spectra with a broad absorption maximum at ca. 583 nm (Figure 5). In comparison to the low-energy  $\pi-\pi^*$  transition in the formazanate aluminum dimethyl compound reported by Sundermeyer ( $\lambda_{\text{max}} = 559$  nm in hexane),<sup>26</sup> compounds **4** and **5** are red-shifted by ca. 25 nm. Comparing diphenyl complex **4** with its boron analogue ( $\lambda_{\text{max}} = 505$  nm)<sup>34</sup> shows that the low-energy band is red-shifted even further. Both observations are consistent with an increase in ionic character for the bonding in **4/5**, due to either the presence of more electron-withdrawing groups on Al (Ph/I vs Me) or a difference in electronegativity of the central element (Al vs B).

**Reduction Chemistry.** Reduction reactions of **1**, **4**, and **5** have been explored. Addition of excess  $\text{Cp}_2\text{Co}$  into a THF solution of **1** results in a color change from dark red to green, a color that is associated with formazanate-centered reductions in boron complexes with this ligand and consistent with formation of the radical anion  $[(\text{PhNNC}(p\text{-tol})\text{NNPh})_2\text{AlCl}]^-$  (**1**<sup>•-</sup>, Scheme 5).<sup>28–30,34</sup> The crude product was washed with hexane and analyzed by EPR spectroscopy. The EPR spectrum of **1**<sup>•-</sup> in fluid THF solution shows a nine-line signal centered at  $g \sim 2$  with a hyperfine coupling constant of 6.35 G (Figure S6). The observed hyperfine coupling pattern indicates that the unpaired electron interacts with 4 (equivalent)  $^{14}\text{N}$  nuclei

( $I = 1$ ), which suggests that it is localized on one of the ligands instead of being delocalized over both formazanates.

The UV/vis spectrum shows two absorptions in the visible range, one at high energy ( $\lambda_{\text{max}} = 426$  nm) and one at low energy ( $\lambda_{\text{max}} = 677$  nm) (Figure S7). Despite the fact that we were unable to obtain analytically pure, crystalline material of **1**<sup>•-</sup>, the EPR and UV/vis spectroscopic features are in agreement with a ligand-based reduction of **1** to form the aluminum-analogue of a verdazyl radical.<sup>56,57</sup> A ligand-centered reduction is further supported by the computational (gas phase DFT) study. The elongation in  $\text{N}-\text{N}$  bonds in **1**<sup>•-</sup> compared to **1** and **1**<sub>calc</sub> (see Table S2) is consistent with the ligand-based reduction as the additional electron populates the ligand  $\text{N}-\text{N}$   $\pi^*$ -orbital.<sup>34</sup> The spin density plot of **1**<sup>•-</sup> indicates the excess spin density is delocalized over both ligands (see Figure S14), a feature that is inconsistent with the EPR spectroscopy (vide supra). This discrepancy is likely due to the fact that the DFT calculations were performed on the isolated anion **1**<sup>•-</sup> in the gas phase. In condensed phase in the presence of counterions, the unpaired electron is likely more localized due to electrostatic interactions: a similar effect is observed in related bis(formazanate) zinc radical anions.<sup>29</sup>

Similarly, treatment of a THF solution of **4** with  $\text{Cp}_2\text{Co}$  results in an immediate color change from intense blue to green, the solution EPR spectrum (Figure S6) of which furnishes a broad signal with  $g$ -value  $\sim 2$ , indicating the formation of  $[\text{Cp}_2\text{Co}]^+[(\text{PhNNC}(p\text{-tol})\text{NNPh})\text{AlPh}_2]^-$  (**4**<sup>•-</sup>, Scheme 6). Similar to the boron analogues of **4**<sup>•-</sup> reported previously,<sup>34</sup> the hyperfine interactions between the unpaired electron and the nitrogen nuclei could not be resolved in this case. Compound **4**<sup>•-</sup> could be obtained in 60% yield as a green powder. The UV/vis spectrum of **4**<sup>•-</sup> shows two absorptions, one at high energy ( $\lambda_{\text{max}} = 460$  nm) and one at low energy ( $\lambda_{\text{max}} = 759$  nm) (Figure S7). The absorptions at 460 and 759 nm are blue- and red-shifted, respectively, compared to the corresponding absorption spectrum found in its parent compound **4** ( $\lambda_{\text{max}} = 583$  nm), which provides evidence for the formation of a formazanate-centered radical.<sup>28–30,34</sup>

Two-electron reduction of **4** was investigated using Na(Hg) as the reducing agent in THF solution, which resulted in a color change from dark blue to orange, via a green transient intermediate (presumably  $4^{\bullet-}$ ). The product  $[(\text{PhNNC}(p\text{-tol})\text{NNPh})\text{AlPh}_2]^{2-}$  ( $4^{2-}$ ) was obtained in crystalline form (42%) as the disodium salt by diffusion of hexane into a DME solution (Scheme 6). Single-crystal structure determination of  $4^{2-}$  reveals that the structure is overall similar to that of the boron analogue reported previously.<sup>34</sup> It shows a distorted tetrahedral geometry around the Al center, which is displaced out of the plane comprised of N1, N2, C7, and N3 atoms from the ligand backbone (i.e., N1N2C7N3-plane) by 0.260 Å (Figure 6). Ligand-based two-electron reduction leads to elongation of the N–N bonds in the ligand backbone to 1.432(2) Å, indicative of a single bond character.<sup>34</sup>

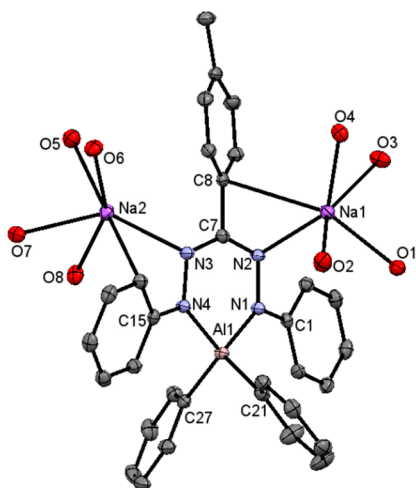


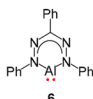
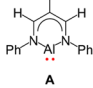
**Figure 6.** Molecular structures of  $4^{2-}$  (right) showing 50% probability ellipsoids. Hydrogen atoms and DME molecules (except for the O atoms bonded to Na) are omitted for clarity.

The 500 MHz  $^1\text{H}$  NMR spectrum for  $4^{2-}$  shows the expected number of resonances for a  $C_{2v}$ -symmetric complex, but the resonances are somewhat broad at room temperature. Variable-temperature measurements indicate this to be due to dynamic processes, the details of which will be described elsewhere. The UV/vis spectrum of  $4^{2-}$  shows an absorption band at 486 nm (Figure S7), which is blue-shifted by 97 nm compared to its precursor **4** ( $\lambda_{\text{max}} = 583$  nm), as expected for a complex with this electron-rich (trianionic) form of the ligand.<sup>34</sup>

Having established two-electron reduction chemistry for diphenyl complex **4**, we turned our attention to diiodide **5**. In this case, reduction would likely be accompanied by loss of halide, similar to what was found before for a formazanate boron difluoride compound.<sup>32</sup> Roesky and co-workers reported that reduction of a ( $\beta$ -diketiminato) aluminum diiodide with 2 equiv of K afforded an unusual low-valent aluminum(I) carbenoid,<sup>25</sup> and its reactivity has been explored in detail in recent years.<sup>58</sup> We were interested to explore whether the (formazanate)Al(I) analogue would be accessible. Treatment of a toluene solution of **5** with 2 equiv of potassium graphite ( $\text{KC}_8$ ) at room temperature resulted in an initial color change from blue to green, which is indicative of the ligand-centered reduction of **5** to verdazyl-type radical  $5^{\bullet-}$ .<sup>28–30,34</sup> The green color faded within 30 min and ultimately a pale blue solution is obtained. Analysis of the crude product by

spectroscopy showed that it was NMR silent, but showed a nine-line signal ( $g \sim 2$ ) in the solution EPR spectrum. All attempts at crystallization of the product(s) were unsuccessful. To probe the nature of the product(s), oxidation of the mixture by addition of  $\text{I}_2$  was carried out to probe whether the starting material could be recovered, but this proved not to be the case. Although the product(s) of two-electron reduction of **5** remain to be identified, we carried out DFT calculations on (formazanate)Al(I) carbenoid (**6**) and compare its electronic structure to Roesky's  $\beta$ -diketiminato analogue. The computational study reveals that the aluminum carbenoid **6** has a singlet ground state with a singlet–triplet energy gap of 11.5 kcal/mol at the B3LYP/6-311G(d,p) level of theory (Table 3).

**Table 3.** Calculated Frontier Orbital Energies and Singlet–Triplet Energy Gaps  $[-(E_S - E_T)]$  for Low-Valent Aluminum Compounds with Formazanate and  $\beta$ -Diketiminato Ligands at the B3LYP/6-311G(d,p) Level of Theory

	$-(E_S - E_T)$ (kcal/mol)	HOMO (eV)	LUMO (eV)	LUMO+1 (eV)
	11.5	-5.25	-3.00	-1.43
	30.7	-4.77	-1.79	-0.80

In case of Roesky's ( $\beta$ -diketiminato)Al(I) complex, it was found that complexes of this type have a singlet–triplet energy gap of ca. 30–35 kcal/mol,<sup>59,60</sup> depending on the ligand substitution pattern. In agreement with the literature, we calculate Roesky's ( $\beta$ -diketiminato)Al complex (with N–Ph substituents; **A** in Table 3) to have a singlet–triplet separation of 30.7 kcal/mol at the B3LYP/6-311G(d,p) level of theory, with the singlet state lowest in energy. Analysis of the frontier orbitals for the  $\beta$ -diketiminato and formazanate compounds shows that in both cases the HOMO is an Al-based lone pair, whereas the LUMO and LUMO+1 are found to be localized on the ligand ( $\pi^*$ ) and the Al center (p-orbital), respectively (Table 3). Although the appearance of the frontier orbitals is similar between the two, the orbital energies are overall lower for the formazanate compound. Of these three frontier orbitals, the formazanate-based  $\pi^*$ -orbital is the most stabilized (1.21 eV lower in energy in **6** than in **A**), whereas the Al-orbitals are shifted in energy by only 0.48–0.63 eV; this accounts for the much lower singlet–triplet separation in **6** than in **A**. From the literature on carbenes (or analogues) of group 13/14 elements, it is apparent that the singlet–triplet energy separation ( $\Delta E_{S-T}$ ) is correlated to reactivity and stability.<sup>43,44,60–63</sup> Thus, although the nitrogen-rich backbone of the formazanate ligand allows tuning of the singlet–triplet gap, the small value obtained for  $\Delta E_{S-T}$  in this case likely results in a system that is too reactive to be isolable.

## CONCLUSIONS

In conclusion, a series of aluminum(III) complexes with redox-active formazanate ligands has been synthesized and

characterized. The five-coordinated bis-formazanate aluminum chloride complex **1** was obtained by the salt metathesis reaction, whereas four-coordinated monoformazanate aluminum diiodide complex **5** was prepared by following a two-step synthetic protocol starting from the free ligands, via corresponding aluminum diphenyl compound **4**. The characterization data for **1**, **4**, and **5**, both in the solid state as well as in solution, provide insights into their electronic and structural properties. In addition, the (electro)chemical reduction of **1**, **4**, and **5** further disclose ligand-centered redox-reactions in these complexes. The possibility to afford (formazanate)Al(I) carbenoid **6** by the two-electron reduction of diiodide complex **5** was investigated by experimental and computational (DFT) studies. The computational data show that in comparison to Roesky's ( $\beta$ -diketiminate)Al(I) complex, the LUMO of the nitrogen-rich formazanate ligand (NNCNN) is significantly stabilized, which results in a computed singlet–triplet energy separation of only 11.5 kcal/mol. The synthesis and characterization data for aluminum complexes with one or two redox-active formazanate ligands reported in this paper provides an entry to studying the reactivity of compounds that combine the electrophilic properties of Al with ligand-based redox activity.

## EXPERIMENTAL SECTION

**General Considerations.** All manipulations were carried out under a nitrogen or an argon atmosphere using standard glovebox, Schlenk, and vacuum-line techniques. Toluene and hexane (Aldrich, anhydrous, 99.8%) were passed over columns of  $\text{Al}_2\text{O}_3$  (Fluka), BASF R3-11-supported Cu oxygen scavenger, and molecular sieves (Aldrich, 4 Å). THF (Aldrich, anhydrous, 99.8%) was dried by percolation over columns of  $\text{Al}_2\text{O}_3$  (Fluka). THF, DME, and hexane were additionally dried on sodium/potassium alloy and subsequently vacuum-transferred and stored under nitrogen. All solvents were degassed prior to use and stored under nitrogen.  $\text{C}_6\text{D}_6$  (Aldrich) and  $d_8$ -THF (Sigma-Aldrich) were vacuum-transferred from sodium/potassium alloy and stored under nitrogen. The ligand PhNNC(*p*-tolyl)NNPh (**LH**)<sup>28</sup> was synthesized according to a published procedure. NMR spectra were recorded on Varian Mercury 400 or Inova 500 spectrometers. The  $^1\text{H}$  and  $^{13}\text{C}$  NMR spectra were referenced internally using the residual solvent resonances and reported in ppm relative to TMS (0 ppm);  $J$  is reported in Hz. Assignments of NMR resonances was aided by COSY, NOESY, HSQC and HMBC experiments using standard pulse sequences. Elemental analyses were performed at the Kolbe Microanalytical Laboratory (Mülheim an der Ruhr, Germany). UV–vis spectra were recorded in toluene, DCE, and THF solution ( $\sim 10^{-3}$  M) in a quartz cuvette that was sealed under  $\text{N}_2$  atmosphere using an AVANTES AvaSpec-2048 spectrometer. Cyclic voltammetry (CV) was performed using a three-electrode configuration comprising a Pt wire counter electrode, a Ag wire pseudoreference electrode and a Pt disk working electrode (CHI102, CH Instruments, diameter = 2 mm). The Pt working electrode was polished before each experiment using an alumina slurry (0.05  $\mu\text{m}$ ) and rinsed (thrice) with distilled water and acetone. The electrodes were then dried in an oven at 75 °C for at least 1 h to remove any residual traces of water. The CV data were referenced by measuring the redox potential of ferrocene, which was added into the solution at the end of the experiment. In all cases, there is no indication that addition of ferrocene influences the electrochemical behavior. All electrochemical measurements were performed at ambient temperatures in a nitrogen glovebox with the compounds dissolved in THF or DME containing 0.1 M [ $^t\text{Bu}_4\text{N}$ ][ $\text{PF}_6$ ] as the supporting electrolyte. The electrochemical data were measured using an Autolab PGSTAT 100 computer-controlled potentiostat with Autolab NOVA software (v.2.1.3).

**Synthesis of [(PhNNC(*p*-tol)NNPh) $_2$ AlCl] (1).** The potassium formazanate salt  $\text{K}[\text{PhNNC}-(p\text{-tol})\text{NNPh}]\cdot 2\text{THF}$  (**LK**) (1.000 g, 2.013 mmol) was dissolved in 30 mL of THF into a double Schlenk flask fitted with a filter. Subsequently, 0.5 equiv of anhydrous  $\text{AlCl}_3$

(0.134 g, 1.007 mmol) was added to this solution. The reaction mixture was stirred for 1 h at room temperature during which the color changed from pink to light red. After that, all volatiles were removed under reduced pressure.  $^1\text{H}$  NMR analysis of the crude product indicates full conversion of the starting materials. The crude product was dissolved again in toluene (30 mL) and filtered to the second tube of the double Schlenk flask. The residue was extracted three times with toluene (30 mL) and the combined filtrate was concentrated in vacuo to ca. 20 mL. Hexane was layered on top of the toluene solution, and after diffusion of the two layers, a solid product precipitated. The supernatant was removed and the residue washed with hexane ( $3 \times 10$  mL) and then dried under vacuum. This gave 250 mg of **1** as dark red crystals (0.360 mmol, 36%). Crystalline material of **1** was also obtained by slow diffusion of hexane into a THF solution of **1**.  $^1\text{H}$  NMR (400 MHz,  $\text{C}_6\text{D}_6$ , 25 °C)  $\delta$  7.93 (d,  $J$  = 8.1 Hz, 4H, *p*-tol *o*-H), 7.58 (d,  $J$  = 7.8 Hz, 8H, NPh *o*-H), 7.14 (d,  $J$  = 8.1 Hz, 4H, *p*-tol *m*-H), 7.02 (t,  $J$  = 7.7 Hz, 8H, NPh *m*-H), 6.94 (t,  $J$  = 7.3 Hz, 4H, NPh *p*-H), 2.20 (s, 6H, *p*-tol- $\text{CH}_3$ ).  $^{27}\text{Al}$  NMR (104 MHz,  $\text{C}_6\text{D}_6$ , 25 °C)  $\delta$  43.0 ( $\gamma_{1/2}$  = 254 Hz).  $^{13}\text{C}$  NMR (100 MHz,  $\text{C}_6\text{D}_6$ , 25 °C)  $\delta$  150.73 (NPh *ipso*-C), 148.32 (NCN), 138.79 (*p*-tol- $\text{CH}_3$  *ipso*-C), 132.95 (NCN-*p*-tol *ipso*-C), 129.42 (*p*-tol *m*-CH), 128.90 (NPh *m*-CH), 127.63 (NPh *p*-CH), 126.50 (*p*-tol *o*-CH), 124.29 (NPh *o*-CH), 21.42 (*p*-tol- $\text{CH}_3$ ). Anal. Calcd for  $\text{C}_{40}\text{H}_{34}\text{AlClN}_4$ : C, 69.71; H, 4.97; N, 16.26. Found: C, 69.82; H, 5.04; N, 16.10.

**Synthesis of [(PhNNC(*p*-tol)NNPh) $_2$ AlCl][Cp $_2$ Co] (1 $^-$ ).** Compound **1** (50 mg, 0.072 mmol) was dissolved in 2 mL of THF, and an excess amount of cobaltocene (55 mg, 0.290 mmol) was added. An immediate color change was observed from dark red to green. The reaction mixture was further stirred for 1 h at room temperature. Addition of 4 mL of hexane precipitated a green powder. Washing the green powder with hexane ( $3 \times 1$  mL) and drying in vacuo afforded 30 mg of **1 $^-$**  as a green powder (0.034 mmol, 47% yield). Satisfactory elemental analysis data could not be obtained.

**Synthesis of [(PhNNC(*p*-tol)NNPh)AlPh $_2$ ] (4).** Free ligand *p*-tolyl-1,5-diphenyl-formazan **LH** (5.000 g, 15.92 mmol) was dissolved in 100 mL of toluene in a Schlenk flask. To this cherry red formazan solution was added a 1 M solution of triphenyl aluminum (17.51 mL, 17.51 mmol) in dibutyl ether at room temperature. The reaction mixture was stirred for 12 h at room temperature, and the color changed from cherry red to dark purple. After this, the solvent was removed under reduced pressure. The  $^1\text{H}$  NMR spectrum of the crude product indicated full conversion of the starting materials and formation of **4**. The crude product was dissolved in toluene and layered with hexane and subsequently crystallized by keeping the solution at  $-30$  °C overnight. The purple crystalline product was washed with hexane ( $3 \times 25$  mL) and dried under vacuum to give **4** as intensely colored pink crystals (6.340 g, 12.820 mmol, 80%).  $^1\text{H}$  NMR (400 MHz,  $\text{C}_6\text{D}_6$ , 25 °C)  $\delta$  8.21 (d,  $J$  = 8.2 Hz, 2H, *p*-tol *o*-H), 7.80 (m, 8H (NPh *o*-H and AlPh *o*-H)), 7.14–7.16 (overlapped, 8H (2H = *p*-tol *m*-H, 6H = AlPh (*m* + *p*)-H)), 6.85 (t,  $J$  = 7.8 Hz, 4H, NPh *m*-H), 6.76 (t,  $J$  = 7.3 Hz, 2H, NPh *p*-H), 2.16 (s, 3H, *p*-tol- $\text{CH}_3$ ).  $^{13}\text{C}$  NMR (100 MHz,  $\text{C}_6\text{D}_6$ , 25 °C)  $\delta$  150.12 (NPh *ipso*-C), 149.33 (NCN), 143.25 (AlPh *ipso*-C), 138.42 (NCN-*p*-tol *ipso*-C), 138.28 (AlPh *o*-CH), 134.92 (*p*-tol- $\text{CH}_3$  *ipso*-C), 129.74 (*p*-tol *m*-CH), 129.28 (NPh *m*-CH), 129.13 (NPh *p*-CH), 128.74 (AlPh *p*-CH), 128.25 (AlPh *m*-CH), 126.30 (*p*-tol *o*-CH), 122.36 (NPh *o*-CH), 21.29 (*p*-tol- $\text{CH}_3$ ). Satisfactory elemental analysis data could not be obtained.

**Synthesis of [(PhNNC(*p*-tol)NNPh)AlPh $_2$ ][Cp $_2$ Co] (4 $^-$ ).** Compound **4** (100 mg, 0.200 mmol) was dissolved in 4 mL of THF, and 1 equiv of cobaltocene (40 mg, 0.200 mmol) was added. An immediate color change was observed from dark purple to green. The reaction mixture was further stirred for 4 h at room temperature. Addition of 4 mL of hexane precipitated a green powder. Washing the green powder with hexane ( $3 \times 2$  mL) and drying in vacuo afforded 85 mg of **4 $^-$**  as a green powder (0.120 mmol, 60% yield). Satisfactory elemental analysis data could not be obtained.

**Synthesis of [(PhNNC(*p*-tol)NNPh)AlPh $_2$ ][Na $_2$ (DME) $_4$ ] (4 $^{2-}$ ).** Compound **4** (200 mg, 0.404 mmol) was dissolved in 7 mL of THF,



Table 4. Crystallographic Data for 1, 4, 4<sup>2-</sup>, and 5

	1	4	4 <sup>2-</sup>	5
chem formula	C <sub>40</sub> H <sub>34</sub> AlClN <sub>8</sub>	C <sub>32</sub> H <sub>27</sub> AlN <sub>4</sub>	C <sub>48</sub> H <sub>67</sub> AlN <sub>4</sub> Na <sub>2</sub> O <sub>8</sub>	C <sub>20</sub> H <sub>17</sub> AlI <sub>2</sub> N <sub>4</sub>
M <sub>r</sub>	689.18	494.55	901.01	594.16
cryst syst	triclinic	Monoclinic	monoclinic	Monoclinic
color, habit	dark red, block	blue, block	orange, block	blue, block
size (mm)	0.15 × 0.12 × 0.08	0.22 × 0.17 × 0.13	0.22 × 0.05 × 0.04	0.31 × 0.13 × 0.05
space group	P $\bar{1}$	C2/c	P2 <sub>1</sub> /c	P2 <sub>1</sub> /c
a (Å)	8.1107(8)	21.5590(14)	13.5694(4)	8.1926(5)
b (Å)	12.0912(12)	15.3001(11)	21.6184(6)	14.8013(9)
c (Å)	18.7007(19)	18.3158(12)	17.2708(5)	17.4444(12)
α (deg)	76.541(4)	90	90	90
β (deg)	87.705(4)	119.229(2)	107.021(2)	97.715(2)
γ (deg)	85.258(4)	90	90	90
V (Å <sup>3</sup> )	1777.0(3)	5272.3(6)	4844.4(2)	2096.2(2)
Z	2	8	4	4
ρ <sub>calc</sub> g·cm <sup>-3</sup>	1.288	1.246	1.231	1.883
radiation [Å]	0.71073	0.71073	1.54178 (Cu)	0.71073
μ(Mo Kα) (mm <sup>-1</sup> )	0.174	0.105		3.055
μ(Cu Kα) (mm <sup>-1</sup> )			0.989	
F(000)	720	2080	1928	1136
temp (K)	100(2)	100(2)	100(2)	100(2)
θ range (deg)	2.951–25.679	2.952–30.583	4.890–70.070	2.964–30.587
data collected (h, k, l)	–9:9, –14:14, –22:22	–30:29, –21:21, –24:26	–16:16, –25:26, –21:21	–11:11, –21:19, –24:24
no. of rflns collected	27047	74978	92849	59061
no. of indepdt rflns	6656	8062	9025	6418
observed rflns F <sub>o</sub> ≥ 2.0 σ(F <sub>o</sub> )	5718	6984	7154	5580
R(F) (%)	7.00	3.72	4.12	2.59
wR(F <sup>2</sup> ) (%)	17.50	10.45	9.10	5.16
GooF	1.141	1.040	1.039	1.089
weighting a, b	0, 8.7365	0.0497, 4.3929	0.0296, 2.9547	0.0155, 3.0472
params refined	453	335	577	245
min, max resid dens	–0.412, 0.676	–0.284, 0.401	–0.260, 0.310	–0.791, 0.829

and 2 equiv of Na(Hg) were added. The reaction mixture was stirred for 12 h, during which it changed its color from dark purple to green and finally orange. Then, the orange solution was filtered through a syringe filter, and the solvent was evaporated under reduced pressure. After that, the crude product was dissolved in 5 mL of DME, and the solution was layered with 5 mL of hexane. Slow diffusion of the two layers at –30 °C precipitated orange crystals, which were washed with pentane (3 × 3 mL) and dried to give compound 4<sup>2-</sup> as a highly air-sensitive solid (155 mg, 0.170 mmol, 42%). <sup>1</sup>H NMR (500 MHz, THF-*d*<sub>6</sub>, –30 °C) δ 8.30 (d, J = 7.8 Hz, 2H, *p*-tol *o*-H), 7.77 (d, J = 7.3 Hz, 4H, AlPh *o*-H), 7.40 (d, J = 7.5 Hz, 2H, N(1)Ph *o*-H), 7.09 (d, J = 7.7 Hz, 2H, *p*-tol *m*-H), 7.01–6.93 (m, 8H, 2H = N(1)Ph *m*-H, 6H = AlPh (*m* + *p*)-H), 6.83 (d, J = 7.9 Hz, 2H, N(2)Ph *o*-H), 6.50 (t, J = 7.0 Hz, 2H, N(2)Ph *m*-H), 5.92 (t, 2H, NPh *p*-H), 3.42 (s, 16H, DME), 3.26 (s, 24H, DME), 2.33 (s, 3H, *p*-tol-CH<sub>3</sub>). <sup>27</sup>Al NMR (104 MHz, THF-*d*<sub>6</sub>, 25 °C) δ 105.0 (γ<sub>1/2</sub> = 1470 Hz). <sup>13</sup>C NMR (125 MHz, THF-*d*<sub>6</sub>, –30 °C) δ 156.31 (NPh *ipso*-C), 154.68 (AlPh *ipso*-C), 150.79 (NCN), 144.59 (NCN-*p*-tol *ipso*-C), 139.53 (AlPh *o*-CH), 135.41 (*p*-tol-CH<sub>3</sub> *ipso*-C), 129.94 (N(1)Ph *m*-CH), 128.11 (*p*-tol (*m* + *o*)-CH), 127.62 (N(2)Ph *m*-CH), 126.64 (AlPh *m*-CH), 125.87 (AlPh *p*-CH), 116.87 (N(1)Ph *o*-CH), 109.89 (NPh *p*-CH), 107.54 (N(2)Ph *o*-CH), 72.71 (DME), 59.01 (DME), 21.43 (*p*-tol-CH<sub>3</sub>). Satisfactory elemental analysis data could not be obtained.

**Synthesis of [(PhNNC(*p*-tol)NNPh)AlI<sub>2</sub>] (5).** Compound 4 (0.700 g, 1.42 mmol) was dissolved in 25 mL of toluene in a Schlenk flask. Subsequently, 2 equiv of I<sub>2</sub> (0.718 g, 2.84 mmol) was added to this dark purple solution. The reaction mixture was stirred for 12 h at room temperature, during which the color faded to light purple. After this the solvent was evaporated under reduced pressure. <sup>1</sup>H NMR analysis of the crude product indicates full conversion of the starting material and formation of 5. The crude product was dissolved

in toluene, layered with hexane, and kept at –30 °C to crystallize. The supernatant was removed and the crystalline solid was washed with hexane (3 × 5 mL) and dried under vacuum to give 590 mg of compound 5 as light pink crystals (0.990 mmol, 70%). <sup>1</sup>H NMR (400 MHz, C<sub>6</sub>D<sub>6</sub>, 25 °C) δ 7.97 (d, J = 8.0 Hz, 6H (2H = *p*-tol *o*-H, 4H = NPh *o*-H)), 7.10 (d, J = 8.0 Hz, 2H, *p*-tol *m*-H), 7.00 (t, J = 7.5 Hz, 4H, NPh *m*-H), 6.94 (t, J = 7.2 Hz, 2H, NPh *p*-H), 2.15 (s, 3H, *p*-tol-CH<sub>3</sub>). <sup>27</sup>Al NMR (104 MHz, C<sub>6</sub>D<sub>6</sub>, 25 °C) δ 69.50 (γ<sub>1/2</sub> = 370 Hz). <sup>13</sup>C NMR (100 MHz, C<sub>6</sub>D<sub>6</sub>, 25 °C) δ 150.33 (NCN), 148.40 (NPh *ipso*-C), 139.23 (NCN-*p*-tol *ipso*-C), 133.55 (*p*-tol-CH<sub>3</sub> *ipso*-C), 129.81 (*p*-tol *m*-CH), 129.72 (NPh *p*-CH), 129.36 (NPh *m*-CH), 126.46 (*p*-tol *o*-CH), 123.46 (NPh *o*-CH), 21.27 (*p*-tol-CH<sub>3</sub>). Anal. Calcd for C<sub>20</sub>H<sub>17</sub>AlN<sub>4</sub>I<sub>2</sub>: C, 40.43; H, 2.88; N, 9.43. Found: C, 40.35; H, 3.06; N, 9.34.

**X-ray Crystallography.** Suitable crystals of compounds 1, 4, and 5 were mounted on top of a cryoloop and transferred into the cold (100 K) nitrogen stream of a Bruker D8 Venture diffractometer. Data collection and reduction was done using the Bruker software suite APEX2.<sup>64</sup> Data collection was carried out at 100 K using either Mo radiation (0.71073 Å) (for 1, 4, and 5) or Cu radiation (1.54178 Å) (for 4<sup>2-</sup>). The final unit cell was obtained from the xyz centroids of 9942 (1), 9860 (4), 9890 (4<sup>2-</sup>), and 9248 (5) reflections after integration. A multiscan absorption correction was applied, based on the intensities of symmetry-related reflections measured at different angular settings (SADABS).<sup>64</sup> The structures were solved by intrinsic phasing methods using SHELXT.<sup>65</sup> The hydrogen atoms were generated by geometrical considerations, constrained to idealized geometries, and allowed to ride on their carrier atoms with an isotropic displacement parameter related to the equivalent displacement parameter of their carrier atoms. Crystal data and details on data collection and refinement are presented in Table 4.

**Computational Studies.** Calculations were performed with the Gaussian09 program<sup>66</sup> using density functional theory (DFT) in the gas phase using the B3LYP functional with 6-311G(d,p) (**1**, **6**, **A**) or 6-311+G(d,p) (**1**<sup>•</sup><sub>cal</sub>) basis set. Geometry optimizations were performed without symmetry constraints, either starting from the X-ray coordinates (**1**) or from structures generated in GaussView 5.0.9.<sup>67</sup> In all cases, the *p*-tolyl group was replaced by Ph for computational efficiency. The geometries of **6** and **A** (both with N-Ph substituents) were optimized on the triplet and singlet surface; broken-symmetry (open-shell singlet) calculations converged on a closed-shell solution. GaussView 5.0.9<sup>67</sup> was used to visualize the computed structures and molecular orbitals.

## ■ ASSOCIATED CONTENT

### ● Supporting Information

The Supporting Information is available free of charge on the ACS Publications website at DOI: [10.1021/acs.inorgchem.9b00553](https://doi.org/10.1021/acs.inorgchem.9b00553).

Experimental details for the synthesis of compounds **2a**, **2b**, **3a**, and **3b**, NMR, EPR, UV/vis spectral data, cyclic voltammograms for compounds **1**, **4** and **5**, computational data, and X-ray crystallographic data (PDF)

### Accession Codes

CCDC 1884433–1884435 and 1899320 contain the supplementary crystallographic data for this paper. These data can be obtained free of charge via [www.ccdc.cam.ac.uk/data\\_request/cif](http://www.ccdc.cam.ac.uk/data_request/cif), or by emailing [data\\_request@ccdc.cam.ac.uk](mailto:data_request@ccdc.cam.ac.uk), or by contacting The Cambridge Crystallographic Data Centre, 12 Union Road, Cambridge CB2 1EZ, UK; fax: +44 1223 336033.

## ■ AUTHOR INFORMATION

### Corresponding Author

\*E-mail: [edwin.otten@rug.nl](mailto:edwin.otten@rug.nl).

### ORCID

Edwin Otten: 0000-0002-5905-5108

### Notes

The authors declare no competing financial interest.

## ■ ACKNOWLEDGMENTS

Financial support from The Netherlands Organisation for Scientific Research (NWO) is gratefully acknowledged (Vidi grant to E.O.). We would like to thank the Center for Information Technology of the University of Groningen for their support and for providing access to the Peregrine high-performance computing cluster. Prof. Wesley Browne and Dr. Juan Chen are acknowledged for help with EPR spectroscopy.

## ■ REFERENCES

- (1) Aldridge, S.; Downs, A. J., Eds. *The Group 13 Metals Aluminium, Gallium, Indium and Thallium: Chemical Patterns and Peculiarities*; John Wiley & Sons, Ltd: Chichester, U.K., 2011.
- (2) Roesky, H. W. The Renaissance of Aluminum Chemistry. *Inorg. Chem.* **2004**, *43*, 7284–7293.
- (3) Chu, T.; Nikonov, G. I. Oxidative Addition and Reductive Elimination at Main-Group Element Centers. *Chem. Rev.* **2018**, *118*, 3608–3680.
- (4) Driess, M.; Nöth, H., Eds. *Molecular Clusters of the Main Group Elements*; Wiley-VCH Verlag GmbH & Co. KGaA: Weinheim, FRG, 2004.
- (5) Bag, P.; Weetman, C.; Inoue, S. Experimental Realisation of Elusive Multiple-Bonded Aluminium Compounds: A New Horizon in Aluminium Chemistry. *Angew. Chem., Int. Ed.* **2018**, *57*, 14394–14413.

(6) Radzewich, C. E.; Guzei, I. A.; Jordan, R. F. Three-Coordinate Cationic Aluminum Alkyl Complexes Incorporating  $\beta$ -Diketiminato Ligands. *J. Am. Chem. Soc.* **1999**, *121*, 8673–8674.

(7) Radzewich, C. E.; Coles, M. P.; Jordan, R. F. Reversible Ethylene Cycloaddition Reactions of Cationic Aluminum  $\beta$ -Diketiminato Complexes. *J. Am. Chem. Soc.* **1998**, *120*, 9384–9385.

(8) Ariafard, A.; Lin, Z.; Jordan, R. F. Theoretical Studies of Cycloaddition Reactions of Cationic Aluminum  $\beta$ -Diketiminato Alkyl Complexes with Alkenes and Alkynes. *Organometallics* **2005**, *24*, 5140–5146.

(9) Dagorne, S.; Atwood, D. A. Synthesis, Characterization, and Applications of Group 13 Cationic Compounds. *Chem. Rev.* **2008**, *108*, 4037–4071.

(10) Jakobsson, K.; Chu, T.; Nikonov, G. I. Hydrosilylation of Olefins Catalyzed by Well-Defined Cationic Aluminum Complexes: Lewis Acid versus Insertion Mechanisms. *ACS Catal.* **2016**, *6*, 7350–7356.

(11) Stender, M.; Eichler, B. E.; Hardman, N. J.; Power, P. P.; Prust, J.; Noltemeyer, M.; Roesky, H. W. Synthesis and Characterization of  $\text{HC}\{\text{C}(\text{Me})\text{N}(\text{C}_6\text{H}_3-2,6\text{-i-Pr}_2)\}_2\text{MX}_2$  (M = Al, X = Cl, I; M = Ga, In, X = Me, Cl, I): Sterically Encumbered  $\beta$ -Diketiminato Group 13 Metal Derivatives. *Inorg. Chem.* **2001**, *40*, 2794–2799.

(12) Qian, B.; Ward, D. L.; Smith, M. R. Synthesis, Structure, and Reactivity of  $\beta$ -Diketiminato Aluminum Complexes. *Organometallics* **1998**, *17*, 3070–3076.

(13) Gong, S.; Ma, H.  $\beta$ -Diketiminato Aluminium Complexes: Synthesis, Characterization and Ring-Opening Polymerization of Cyclic Esters. *Dalton. Trans.* **2008**, *0*, 3345.

(14) Yang, Y.; Schulz, T.; John, M.; Ringe, A.; Roesky, H. W.; Stalke, D.; Magull, J.; Ye, H. Synthesis, Characterization, and Reaction of Aluminum Halide Amides Supported by a Bulky  $\beta$ -Diketiminato Ligand. *Inorg. Chem.* **2008**, *47*, 2585–2592.

(15) Bai, G.; Peng, Y.; Roesky, H. W.; Li, J.; Schmidt, H.-G.; Noltemeyer, M. Aluminum Dihydroxide with Terminal OH Groups: An Unprecedented Congener of Boronic Acid. *Angew. Chem., Int. Ed.* **2003**, *42*, 1132–1135.

(16) Yang, Y.; Li, H.; Wang, C.; Roesky, H. W. Studies of the Ligand Effect on the Synthesis of Dialuminumoxanes by Various  $\beta$ -Diketiminato Ligands. *Inorg. Chem.* **2012**, *51*, 2204–2211.

(17) Bai, G.; Singh, S.; Roesky, H. W.; Noltemeyer, M.; Schmidt, H.-G. Mononuclear Aluminum Hydroxide for the Design of Well-Defined Homogeneous Catalysts. *J. Am. Chem. Soc.* **2005**, *127*, 3449–3455.

(18) Yang, Y.; Schulz, T.; John, M.; Yang, Z.; Jiménez-Pérez, V. M.; Roesky, H. W.; Gurubasavaraj, P. M.; Stalke, D.; Ye, H. Organoaluminum Hydroxides Supported by  $\beta$ -Diketiminato Ligands: Synthesis, Structural Characterization, and Reactions. *Organometallics* **2008**, *27*, 769–777.

(19) Chai, J.; Jancik, V.; Singh, S.; Zhu, H.; He, C.; Roesky, H. W.; Schmidt, H.-G.; Noltemeyer, M.; Hosmane, N. S. Synthesis of a New Class of Compounds Containing a Ln–O–Al Arrangement and Their Reactions and Catalytic Properties. *J. Am. Chem. Soc.* **2005**, *127*, 7521–7528.

(20) Li, D.; Peng, Y.; Geng, C.; Liu, K.; Kong, D. Well-Controlled Ring-Opening Polymerization of Cyclic Esters Initiated by Dialkylaluminum  $\beta$ -Diketiminates. *Dalton. Trans.* **2013**, *42*, 11295.

(21) Ma, X.; Yao, M.; Zhong, M.; Deng, Z.; Li, W.; Yang, Z.; Roesky, H. W. Synthesis and Characterization of  $\beta$ -Diketiminato Aluminum Compounds and Their Use in the Ring-Opening Polymerization of  $\epsilon$ -Caprolactone. *Z. Anorg. Allg. Chem.* **2017**, *643*, 198–202.

(22) Uhl, W.; Jana, B. A Persistent Alkylaluminum Peroxide: Surprising Stability of a Molecule with Strong Reducing and Oxidizing Functions in Close Proximity. *Chem. - Eur. J.* **2008**, *14*, 3067–3071.

(23) Uhl, W.; Jana, B. Reactions of  $\beta$ -Diketiminatoaluminum Hydrides with Tert-Butyl Hydrogenperoxide – Facile Formation of Dialuminumoxanes Containing Al–O–Al Groups. *J. Organomet. Chem.* **2009**, *694*, 1101–1106.

- (24) Jana, B.; Uhl, W. New Aluminum and Gallium Complexes of  $\beta$ -Diketiminato and  $\beta$ -Ketiminato Ligands. *Inorg. Chim. Acta* **2017**, *455*, 61–69.
- (25) Cui, C.; Roesky, H. W.; Schmidt, H.-G.; Noltemeyer, M.; Hao, H.; Cimpoesu, F. Synthesis and Structure of a Monomeric Aluminum(I) Compound [ $\{HC(CMeNAr)_2\}Al$ ] (Ar = 2,6- $iPr_2C_6H_3$ ): A Stable Aluminum Analogue of a Carbene. *Angew. Chem., Int. Ed.* **2000**, *39*, 4274–4276.
- (26) Schorn, W.; Grosse-Hagenbrock, D.; Oelkers, B.; Sundermeyer, J. Formazanido Complexes of Heavier Group 13 Elements Aluminium, Gallium, and Indium. *Dalton. Trans.* **2016**, *45*, 1201–1207.
- (27) Maar, R. R.; Rabiee Kenaree, A.; Zhang, R.; Tao, Y.; Katzman, B. D.; Staroverov, V. N.; Ding, Z.; Gilroy, J. B. Aluminum Complexes of  $N_2O_2^{3-}$  Formazanate Ligands Supported by Phosphine Oxide Donors. *Inorg. Chem.* **2017**, *56*, 12436–12447.
- (28) Gilroy, J. B.; Ferguson, M. J.; McDonald, R.; Patrick, B. O.; Hicks, R. G. Formazans as  $\beta$ -Diketiminato Analogues. Structural Characterization of Boratetrazines and Their Reduction to Borataverdazyl Radical Anions. *Chem. Commun.* **2007**, *0*, 126–128.
- (29) Chang, M. C.; Dann, T.; Day, D. P.; Lutz, M.; Wildgoose, G. G.; Otten, E. The Formazanate Ligand as an Electron Reservoir: Bis(Formazanate) Zinc Complexes Isolated in Three Redox States. *Angew. Chem., Int. Ed.* **2014**, *53*, 4118–4122.
- (30) Chang, M.-C.; Otten, E. Synthesis and Ligand-Based Reduction Chemistry of Boron Difluoride Complexes with Redox-Active Formazanate Ligands. *Chem. Commun.* **2014**, *50*, 7431–7433.
- (31) Chang, M.-C.; Roewen, P.; Travieso-Puente, R.; Lutz, M.; Otten, E. Formazanate Ligands as Structurally Versatile, Redox-Active Analogues of  $\beta$ -Diketiminates in Zinc Chemistry. *Inorg. Chem.* **2015**, *54*, 379–388.
- (32) Chang, M.-C.; Otten, E. Reduction of (Formazanate)Boron Difluoride Provides Evidence for an N-Heterocyclic B(I) Carbenoid Intermediate. *Inorg. Chem.* **2015**, *54*, 8656–8664.
- (33) Chang, M. C.; Chantzis, A.; Jacquemin, D.; Otten, E. Boron Difluorides with Formazanate Ligands: Redox-Switchable Fluorescent Dyes with Large Stokes Shifts. *Dalton. Trans.* **2016**, *45*, 9477–9484.
- (34) Mondol, R.; Snoeken, D. A.; Chang, M.-C.; Otten, E. Stable, Crystalline Boron Complexes with Mono-, Di- and Trianionic Formazanate Ligands. *Chem. Commun.* **2017**, *53*, 513–516.
- (35) Barbon, S. M.; Reinkeluers, P. A.; Price, J. T.; Staroverov, V. N.; Gilroy, J. B. Structurally Tunable 3-Cyanoformazanate Boron Difluoride Dyes. *Chem. - Eur. J.* **2014**, *20*, 11340–11344.
- (36) Barbon, S. M.; Price, J. T.; Reinkeluers, P. A.; Gilroy, J. B. Substituent-Dependent Optical and Electrochemical Properties of Triarylformazanate Boron Difluoride Complexes. *Inorg. Chem.* **2014**, *53*, 10585–10593.
- (37) Barbon, S. M.; Price, J. T.; Yogarajah, U.; Gilroy, J. B. Synthesis and Characterization of Conjugated/Cross-Conjugated Benzene-Bridged Boron Difluoride Formazanate Dimers. *RSC Adv.* **2015**, *5*, 56316–56324.
- (38) Maar, R. R.; Barbon, S. M.; Sharma, N.; Groom, H.; Luyt, L. G.; Gilroy, J. B. Evaluation of Anisole-Substituted Boron Difluoride Formazanate Complexes for Fluorescence Cell Imaging. *Chem. - Eur. J.* **2015**, *21*, 15589–15599.
- (39) Hesari, M.; Barbon, S. M.; Staroverov, V. N.; Ding, Z.; Gilroy, J. B. Efficient Electrochemiluminescence of a Readily Accessible Boron Difluoride Formazanate Dye. *Chem. Commun.* **2015**, *51*, 3766–3769.
- (40) Barbon, S. M.; Staroverov, V. N.; Gilroy, J. B. Effect of Extended  $\pi$  Conjugation on the Spectroscopic and Electrochemical Properties of Boron Difluoride Formazanate Complexes. *J. Org. Chem.* **2015**, *80*, 5226–5235.
- (41) Barbon, S. M.; Buddingh, J. V.; Maar, R. R.; Gilroy, J. B. Boron Difluoride Adducts of a Flexidentate Pyridine-Substituted Formazanate Ligand: Property Modulation via Protonation and Coordination Chemistry. *Inorg. Chem.* **2017**, *56*, 12003–12011.
- (42) Barbon, S. M.; Staroverov, V. N.; Gilroy, J. B. Structurally Diverse Boron-Nitrogen Heterocycles from an  $N_2O_2^{3-}$  Formazanate Ligand. *Angew. Chem., Int. Ed.* **2017**, *56*, 8173.
- (43) Frey, G. D.; Lavallo, V.; Donnadiu, B.; Schoeller, W. W.; Bertrand, G. Facile Splitting of Hydrogen and Ammonia by Nucleophilic Activation at a Single Carbon Center. *Science* **2007**, *316*, 439–441.
- (44) Protchenko, A. V.; Bates, J. L.; Saleh, L. M. A.; Blake, M. P.; Schwarz, A. D.; Kolychev, E. L.; Thompson, A. L.; Jones, C.; Mountford, P.; Aldridge, S. Enabling and Probing Oxidative Addition and Reductive Elimination at a Group 14 Metal Center: Cleavage and Functionalization of E-H Bonds by a Bis(Boryl)Stannylenes. *J. Am. Chem. Soc.* **2016**, *138*, 4555–4564.
- (45) Travieso-Puente, R.; Chang, M. C.; Otten, E. Alkali Metal Salts of Formazanate Ligands: Diverse Coordination Modes as a Result of the Nitrogen-Rich [NNCNN] Ligand Backbone. *Dalton. Trans.* **2014**, *43*, 18035–18041.
- (46) Addison, A. W.; Rao, T. N.; Reedijk, J.; van Rijn, J.; Verschoor, G. C. Synthesis, Structure, and Spectroscopic Properties of Copper(II) Compounds Containing Nitrogen-sulphur Donor Ligands; the Crystal and Molecular Structure of Aqua[1,7-Bis(N-Methylbenzimidazol-2'-yl)-2,6-Dithiaheptane]Copper(II) Perchlorate. *J. Chem. Soc., Dalton Trans.* **1984**, *2*, 1349–1356.
- (47) Myers, T. W.; Kazem, N.; Stoll, S.; Britt, R. D.; Shanmugam, M.; Berben, L. A. A Redox Series of Aluminum Complexes: Characterization of Four Oxidation States Including a Ligand Biradical State Stabilized via Exchange Coupling. *J. Am. Chem. Soc.* **2011**, *133*, 8662–8672.
- (48) Moilanen, J.; Borau-Garcia, J.; Roesler, R.; Tuononen, H. M. Paramagnetic Aluminium  $\beta$ -Diketiminato. *Chem. Commun.* **2012**, *48*, 8949.
- (49) Berry, R. S. Correlation of Rates of Intramolecular Tunneling Processes, with Application to Some Group V Compounds. *J. Chem. Phys.* **1960**, *32*, 933–938.
- (50) Alemany, L. B.; Kirker, G. W. First Observation of 5-Coordinate Aluminum by MAS  $^{27}Al$  NMR in Well-Characterized Solids. *J. Am. Chem. Soc.* **1986**, *108*, 6158–6162.
- (51) Gilson, J.-P.; Edwards, G. C.; Peters, A. W.; Rajagopalan, K.; Wormsbecher, R. F.; Roberie, T. G.; Shatlock, M. P. Penta-Coordinated Aluminium in Zeolites and Aluminosilicates. *J. Chem. Soc., Chem. Commun.* **1987**, No. 2, 91.
- (52) Lambert, J. F.; Millman, W. S.; Fripiat, J. J. Revisiting Kaolinite Dehydroxylation: A  $^{29}Si$  and  $^{27}Al$  MAS NMR Study. *J. Am. Chem. Soc.* **1989**, *111*, 3517–3522.
- (53) Massiot, D.; Kahn-Harari, A.; Michel, D.; Muller, D.; Taulelle, F. Aluminium-27 MAS NMR of  $Al_2Ge_2O_7$  and  $LaAlGe_2O_7$ : Two Pentacoordinated Aluminium Environments. *Magn. Reson. Chem.* **1990**, *28*, S82–S88.
- (54) Yang, Y.; Schulz, T.; John, M.; Ringe, A.; Roesky, H. W.; Stalke, D.; Magull, J.; Ye, H. Synthesis, Characterization, and Reaction of Aluminum Halide Amides Supported by a Bulky  $\beta$ -Diketiminato Ligand. *Inorg. Chem.* **2008**, *47*, 2585–2592.
- (55) Cui, C.; Roesky, H. W.; Noltemeyer, M.; Lappert, M. F.; Schmidt, H.-G.; Hao, H. Synthesis and Structures of Mono(1-Aza-Allyl) Complexes of Aluminum. *Organometallics* **1999**, *18*, 2256–2261.
- (56) Hicks, R. G. Verdazyls and Related Radicals Containing the Hydrazyl [ $R_2N-NR$ ] Group. In *Stable Radicals*; John Wiley & Sons, Ltd: Chichester, U.K., 2010; pp 245–279.
- (57) Matuschek, D.; Eusterwiemann, S.; Stegemann, L.; Doerenkamp, C.; Wibbeling, B.; Daniliuc, C. G.; Doltsinis, N. L.; Strassert, C. A.; Eckert, H.; Studer, A. Profluorescent Verdazyl Radicals – Synthesis and Characterization. *Chem. Sci.* **2015**, *6*, 4712–4716.
- (58) Chu, T.; Nikonov, G. I. Oxidative Addition and Reductive Elimination at Main-Group Element Centers. *Chem. Rev.* **2018**, *118*, 3608–3680.
- (59) Schoeller, W. W. Neutral Carbene Analogues of Group 13 Elements: The Dimerization Reaction to a Biradicaloid. *Inorg. Chem.* **2011**, *50*, 2629–2633.
- (60) Reiher, M.; Sundermann, A. Do Divalent [ $\{HC(CR'NR'')_2\}E$ ] Compounds Contain E(I) or E(III) (E = B, Al, Ga, In)? On the

Correspondence of Formal Oxidation Numbers, Lewis Structures, and Reactivity. *Eur. J. Inorg. Chem.* **2002**, *2002*, 1854–1863.

(61) Chen, C.-H.; Tsai, M.-L.; Su, M.-D. Theoretical Study of the Reactivities of Neutral Six-Membered Carbene Analogues of the Group 13 Elements. *Organometallics* **2006**, *25*, 2766–2773.

(62) Peng, Y.; Ellis, B. D.; Wang, X.; Power, P. P. Diarylstannylyene Activation of Hydrogen or Ammonia with Arene Elimination. *J. Am. Chem. Soc.* **2008**, *130*, 12268–12269.

(63) Wang, Y.; Ma, J. Silylenes and Germynes: The Activation of H-H Bond in Hydrogen Molecule. *J. Organomet. Chem.* **2009**, *694*, 2567–2575.

(64) APEX2, v2012.4–3; SAINT, version 8.18C, SADABS, version 2012/1; Bruker AXS Inc.: Madison, WI, 2012.

(65) Sheldrick, G. M. SHELXT - Integrated Space-Group and Crystal-Structure Determination. *Acta Crystallogr., Sect. A: Found. Adv.* **2015**, *71*, 3–8.

(66) Frisch, M. J.; Trucks, G. W.; Schlegel, H. B.; Scuseria, G. E.; Robb, M. A.; Cheeseman, J. R.; Scalmani, G.; Barone, V.; Mennucci, B.; Petersson, G. A.; Nakatsuji, H.; Caricato, M.; Li, X.; Hratchian, H. P.; Izmaylov, A. F.; Bloino, J.; Zheng, G.; Sonnenberg, J. L.; Hada, M.; Ehara, M.; Toyota, K.; Fukuda, R.; Hasegawa, J.; Ishida, M.; Nakajima, T.; Honda, Y.; Kitao, O.; Nakai, H.; Vreven, T.; Montgomery, J. A., Jr.; Peralta, J. E.; Ogliaro, F.; Bearpark, M.; Heyd, J. J.; Brothers, E.; Kudin, K. N.; Staroverov, V. N.; Kobayashi, R.; Normand, J.; Raghavachari, K.; Rendell, A.; Burant, J. C.; Iyengar, S. S.; Tomasi, J.; Cossi, M.; Rega, N.; Millam, J. M.; Klene, M.; Knox, J. E.; Cross, J. B.; Bakken, V.; Adamo, C.; Jaramillo, J.; Gomperts, R.; Stratmann, R. E.; Yazyev, O.; Austin, A. J.; Cammi, R.; Pomelli, C.; Ochterski, J. W.; Martin, R. L.; Morokuma, K.; Zakrzewski, V. G.; Voth, G. A.; Salvador, P.; Dannenberg, J. J.; Dapprich, S.; Daniels, A. D.; Farkas, O.; Foresman, J. B.; Ortiz, J. V.; Cioslowski, J.; Fox, D. J. *Gaussian 09*, revision D.01; Gaussian, Inc.: Wallingford, CT, 2009.

(67) Dennington, R.; Keith, T.; Millam, J. *GaussView*, version 5; Semichem Inc.: Shawnee Mission, KS, 2009.